



The Intensity and Evolution of the Extreme Solar and Geomagnetic Storms in 1938 January

Hisashi Hayakawa^{1,2,3,4} , Kentaro Hattori⁵ , Alexei A. Pevtsov^{6,7} , Yusuke Ebihara⁸ , Margaret A. Shea⁹,
Ken G. McCracken¹⁰ , Ioannis A. Daglis^{11,12} , Ankush T. Bhaskar^{13,14} , Paulo Ribeiro¹⁵ , and Delores J. Knipp^{16,17}

¹Institute for Space-Earth Environmental Research, Nagoya University, Nagoya, 4648601, Japan; hisashi@nagoya-u.jp

²Institute for Advanced Researches, Nagoya University, Nagoya, 4648601, Japan

³UK Solar System Data Centre, Space Physics and Operations Division, RAL Space, Science and Technology Facilities Council, Rutherford Appleton Laboratory, Harwell Oxford, Didcot, Oxfordshire, OX11 0QX, UK

⁴Nishina Centre, Riken, Wako, 3510198, Japan

⁵Graduate School of Science, Kyoto University, Kyoto, 6068501, Japan

⁶National Solar Observatory, 3665 Discovery Drive, 3rd Floor, Boulder, CO 80303, USA

⁷Central Astronomical observatory of Russian Academy of Sciences at Pulkovo, Saint Petersburg, 196140, Russia

⁸Research Institute for Sustainable Humanosphere, Kyoto University, Uji, 6110011, Japan

⁹SSSRC, 100 Tennyson Avenue, Nashua, NH 03062, USA

¹⁰64 Burradoo Road, Burradoo, 2576, NSW, Australia

¹¹Department of Physics, National and Kapodistrian University of Athens, Athens, 15784, Greece

¹²Hellenic Space Center, Athens, 15231, Greece

¹³NASA Goddard Space Flight Center, Greenbelt, MD, USA

¹⁴Space Physics Laboratory, Vikram Sarabhai Space Centre, ISRO, Thiruvananthapuram-695022, Kerala, India

¹⁵University of Coimbra, CITEUC, Geophysical and Astronomical Observatory, Coimbra, 3040-004, Portugal

¹⁶Smead Aerospace Engineering Sciences Department, University of Colorado Boulder, Boulder, CO 80309, USA

¹⁷High Altitude Observatory, National Center for Atmospheric Research, Boulder, CO 80307, USA

Received 2020 September 10; revised 2020 October 18; accepted 2020 October 21; published 2021 March 17

Abstract

Major solar eruptions occasionally direct interplanetary coronal mass ejections (ICMEs) to Earth and cause significant geomagnetic storms and low-latitude aurorae. While individual extreme storms are significant threats to modern civilization, storms occasionally appear in sequence, acting synergistically, and cause “perfect storms” on Earth. The stormy interval in 1938 January was one of such cases. Here, we analyze the contemporary records to reveal its time series on their source active regions, solar eruptions, ICMEs, geomagnetic storms, low-latitude aurorae, and cosmic-ray (CR) variations. Geomagnetic records show that three storms occurred successively on January 17/18 ($D_{cx} \approx -171$ nT), January 21/22 ($D_{cx} \approx -328$ nT), and January 25/26 ($D_{cx} \approx -336$ nT). The amplitudes of the CR variations and storm sudden commencements (SSCs) show the impact of the first ICME as the largest ($\approx 6\%$ decrease in CR and 72 nT in SSC) and the ICMEs associated with the storms that followed as more moderate ($\approx 3\%$ decrease in CR and 63 nT in SSC; $\approx 2\%$ decrease in CR and 63 nT in SSC). Interestingly, a significant solar proton event occurred on January 16/17 and the Cheltenham ionization chamber showed a possible ground-level enhancement. During the first storm, aurorae were less visible at midlatitudes, whereas, during the second and third storms, the equatorward boundaries of the auroral oval were extended down to 40.3° and 40.0° in invariant latitude. This contrast shows that the initial ICME was probably faster, with a higher total magnitude but a smaller southward component.

Unified Astronomy Thesaurus concepts: [Solar flares \(1496\)](#); [Solar coronal mass ejections \(310\)](#); [Geomagnetic fields \(646\)](#); [Sunspots \(1653\)](#); [Solar active regions \(1974\)](#); [Solar-terrestrial interactions \(1473\)](#); [Solar energetic particles \(1491\)](#); [Forbush effect \(546\)](#); [Cosmic rays \(329\)](#)

1. Introduction

Large and complex sunspot groups occasionally trigger solar flares and launch sequential coronal mass ejections (CMEs) into space, where they are identified as interplanetary coronal mass ejections (ICMEs; Gopalswamy et al. 2005; Tsurutani et al. 2014; Liu et al. 2019). ICMEs with a southward magnetic field component that impact Earth typically initiate a significant geospace magnetic storm with an equatorward expansion of the auroral oval (Gonzalez et al. 1994; Yokoyama et al. 1998; Daglis et al. 1999; Gopalswamy et al. 2007).

The intensity of geomagnetic storms has been measured through the disturbance storm time (Dst) index, as a proxy of the terrestrial ring-current intensity, on the basis of variability of the horizontal intensity of four midlatitude stations with geomagnetic latitudinal weighting: Kakioka, Hermanus, San Juan, and Honolulu (Sugiura 1964; Gonzalez et al. 1994; Daglis et al. 1999; Daglis 2006; WDC for Geomagnetism at

Kyoto et al. 2015). Since the beginning of the Dst index measurement in 1957, the largest geomagnetic storm was recorded in 1989 March (with a record value of most negative $Dst = -589$), during which significant low-latitude aurorae and serious blackouts were recorded (Allen et al. 1989; Boteler 2019). Extending our investigations back to the beginning of systematic magnetic measurements in the mid-19th century, we note other intense geomagnetic storms such as those in 1859 September, 1872 February, and 1921 May (Tsurutani et al. 2003; Silverman 2006; Cliver & Dietrich 2013; Hayakawa et al. 2016, 2018, 2019, 2020c; Hapgood 2019; Love et al. 2019).

Understanding such intense solar and geomagnetic storms is more than just an academic concern, as the occurrence of such storms represents a significant risk to modern civilization, because of our increasing dependency on technology-based infrastructure that is vulnerable to various aspects of such solar

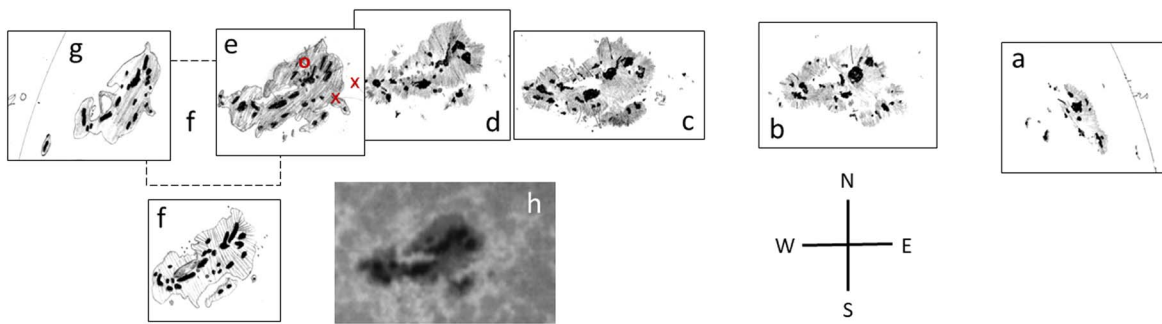


Figure 1. Evolution of AR MWO 5726 during its disk passage in 1938 January: (a) January 13, 17:50 UT, (b) January 16, 16:20 UT, (c) January 18, 16:15 UT, (d) January 19, 19:00 UT, (e) January 20, 11:30 UT, (f) January 21, 19:45 AM, (g) January 22, 19:10 UT, and (h) spectroheliogram in Ca K1 for the location corresponding to panel (d) on January 19. The locations of panels (a)–(g) correspond to their heliographic coordinates on the solar disk for the day of observation. The diameter of solar disk can be inferred from the position of solar limbs shown in panels (a) and (g). Panel (f) is shifted from its true location (shown as a dashed square). Red crosses in panel (e) mark the location of two bright H α kernels, and the red circle is the location of large Doppler velocity measured in H α , both measured at 00:00 UT (January 21). The measured Doppler shift (2 \AA) corresponds to the Doppler velocity of $\approx 90 \text{ km s}^{-1}$.

and geomagnetic storms. Among them, the 1989 March storm and other major storms have seriously affected human civilization with their resultant geomagnetically induced currents (e.g., Allen et al. 1989; Boteler 2019). The modern expected consequences of the superstorms in 1859 September and 1921 May have been considered even more catastrophic and have been studied intensively (Daglis 2001, 2005; Baker et al. 2008; Hapgood 2018; Riley et al. 2018).

Such ICMEs may become even more geo-effective when a series of them are launched from a single source sunspot active region (AR). For such a sequence of events, initial ICMEs sweep the interplanetary space allowing the following ICMEs to decelerate less (Tsurutani & Lakhina 2014; Tsurutani et al. 2014; Shiota & Kataoka 2016). This was the case with the Halloween sequence in 2003 October (Gopalswamy et al. 2005; Mannucci et al. 2005; Shiota & Kataoka 2016). Close inspections of the time series of the extreme storms and superstorms show that they occasionally consist of multiple storms within several days (e.g., Silverman 2006; Cid et al. 2014; Knipp et al. 2016; Lefèvre et al. 2016; Boteler 2019; Hayakawa et al. 2017, 2019; Hattori et al. 2019; Love et al. 2019).

The geomagnetic storm on 1938 January 25 was one of such cases. Its intensity was ranked 10th in the observations of Greenwich-Abinger magnetograms in 1874–1954 (Jones 1955, p. 79) and 33rd in the *aa* index in 1868–2010 (Lefèvre et al. 2016). It was also accompanied by a splendid auroral display throughout Europe even down to Gibraltar, Sicily, and Greece (Störmer 1938; Anon 1938; Carapiperis 1956; Correia & Ribeiro 1996), and a series of global decreases in the cosmic-ray (CR) intensity (Forbush decreases) detected by ionization chambers (ICs; Forbush 1938; Hess et al. 1938). The January 25 storm was the third in a sequence of events that produced four sudden impulses, three of which created the SSC and associated geomagnetic storms in a 9 day interval. Among them, two storms on January 21/22 with less intensity and January 25/26 with a higher intensity, have been highlighted as twin occurrences with great auroral displays and have been compared to the superstorms around the Carrington event in 1859 August and September (Silverman 2006, see also Hayakawa et al. 2019).

Since these geomagnetic storms occurred long before the development of the Dst index in 1957, these events and the time series of the associated solar and terrestrial phenomena have been in need of quantitative evaluations and detailed

analyses to be compared with the major storms during the modern instrumental observations. Therefore, in this article, we have aimed at reconstructing their time series from onset at the source AR, characterizing the source flares and ICMEs, to the intensity and time series of the geomagnetic storms, the low-latitude aurorae, and the solar CR variability, on the basis of the contemporary observational records.

2. Solar Eruptions

Solar Cycle 17 reached its maximum in 1937 April (Table 1 of Hathaway 2015, Figure 2 of Clette & Lefèvre 2016), culminating in a giant sunspot group crossing the solar central meridian on April 24. The sunspot activity has been regularly monitored at the initial observatories such as the Mount Wilson Observatory (e.g., Pevtsov et al. 2019) and Tashkent Observatory (Slonim & Ushakova 1938; Slonim 1939) around this period and recorded as daily sunspot magnetic field measurements and daily sunspot drawings. On this basis, over the following 8–9 months, the sunspot activity went through multiple episodes of enhanced-diminished activity with several giant sunspots visible with a naked eye forming mostly in the northern solar hemisphere. Thus, for example, the sunspot activity had weakened in 1937 May, but by mid-June, several ARs begun developing in both solar hemispheres. On 1937 July 29, a sunspot group with two giant naked-eye sunspots situated in the northern solar hemisphere crossed the central meridian. Over the following months, the activity had weakened again. Another giant sunspot group had developed in the northern solar hemisphere and crossed the central meridian around 1937 October 4, and then again, November–December was relatively calm in its sunspot activity. Disk passage of the giant spots, which developed during this 8 month period was accompanied by major geomagnetic storms. In 1937, the sunspot activity exhibited strong hemispheric asymmetry, with the Northern hemisphere being the most active. Interestingly, the majority of giant sunspot groups that were observed on the Sun in 1937 had developed in the range of antipodal Carrington longitudes of 175° – 195° and 350° – 355° (Moisejev 1939a), which may be associated with solar active longitude (e.g., Becker 1955; Bumba & Howard 1965; Haurwitz 1968; Berdyugina & Usoskin 2003; Sudol & Harvey 2005; Usoskin et al. 2007). A giant sunspot AR RGO¹⁸ 12673 (MWO¹⁹ 5726) appeared on the solar disk at the

¹⁸ Royal Greenwich Observatory.

¹⁹ Mount Wilson Observatory.

east limb in the Northern hemisphere on January 12. It crossed the central meridian on January 18, and disappeared behind the West limb on January 24 (Figure 1). This was the seventh largest sunspot region by mean area between 1874–1954 (Jones 1955) and was a recurrent region, existing over three consecutive solar rotations. The Carrington longitudinal position of this region was close to one of the “active longitudes” that produced a number of giant sunspots in 1937. The AR grew to 3627 millionths of the solar hemisphere (msh).²⁰ The main sunspot of this group was a shapeless conglomerate of multiple umbrae with the opposite polarity magnetic fields surrounded by a common penumbra and had area of about 3361 msh (Slonim & Ushakova 1938; Kurochkin 1939; Moisejev 1939a; Slonim 1939, see the daily sunspot magnetic field observations and daily sunspot drawings at the Mount Wilson Observatory (e.g., Pevtsov et al. 2019)).

During its disk passage, this AR produced a number of solar flares including four major flares with their $H\alpha$ importance = 3 as well as numerous weaker flares of importance 1 and 2, as recorded in *Quarterly Bulletin of Solar Activity* (hereafter QBSA) (D’Azambuja 1938, p. 124). Note that this importance indicates the $H\alpha$ flaring area; 1 = 100–250 msh; 2 = 250–600 msh; and 3 = 600–1200 msh (see Švestka 1976, p. 14), whereas the relative brightness has been annotated with B for bright, N for normal, and F for faint. Optical flares in $H\alpha$ are usually accompanied by radio and X-ray bursts, and occasionally by high-energy particle emissions.

So far we have at least four major $H\alpha$ flares (=class 3) in this interval. The first major flare was observed on January 14 at around 04:40–05:30 UT with a spectroheliograph at Watheroo, when this AR was positioned at N10E45 (south of the main sunspot). The second major flare was observed on January 20 at around 18:20–21:27 UT at Mount Wilson, when this AR was positioned at N18W30. The maximum of $H\alpha$ flare was recorded at 19:52 UT. The third and fourth major flares²¹ were observed on 1938 January 24: one during 03:00–03:40 UT according to Watheroo observations and the other at around 05:12–07:00 UT based on spectroheliograph observations from Canberra from the AR at N22W85 to N22W80. The fourth major flare on January 24 is especially noted as “in connection with an eruptive protuberance” (D’Azambuja 1938, p. 124). As their flare importance were classified as 3, it is considered that the flare area in $H\alpha$ reached 600–1200 msh (e.g., Švestka 1976, p. 14). Moreover, it is quite possible that not all the flare activities from this region were recorded in the QBSA. Thus, for example, MWO drawing taken on January 21 (Figure 1, panel (e)) contains notes about two bright $H\alpha$ kernels, as well as a measurement of a significant shift in $H\alpha$ spectral line. The shift corresponds to a significant (90 km s^{-1}) Doppler velocity consistent with an eruptive event. The time of these measurements (00UT on January 21) is about 4 hr after the last eruptive event on January 20 and about 2 hr before the first eruptive event on January 21 listed in the QBSA. Thus, it must be a different flare of unknown importance.

Given the strength (importance) of optical ($H\alpha$) flares in AR MWO 5726, there is a high probability that this region produced major X-ray flares. For example, Hayakawa et al. (2020a) used NOAA lists of flares to demonstrate that in 96% cases, the H-alpha flare of importance 3 is accompanied with either X-class (66%) or M-class (30%) flares. Major X-ray

(X- and M-class) flares are almost always accompanied with ICMEs, as shown from the statistical studies with the LASCO (Large Angle and Spectrometric Coronagraph; Brueckner et al. 1995) observations on the Solar and Heliospheric Observatory (Domingo et al. 1995) mission during 1996–2010 (Youssef 2012) 90% of all X-class flares and 30% of all M-class flares are accompanied by ICMEs. Indeed, shortly after these flares, three storm sudden commencements (SSCs) with significant amplitudes were recorded on January 16 (22:36 UT, 72 nT), January 22 (02:42 UT, 63 nT), and January 25 (11:51 UT, 63 nT) at the Kakioka Observatory.²² Their time lags show that these ICMEs responsible for these SSCs reached the Earth 65.9, 30.3, and 32.9 hr, respectively, after the occurrence of the $H\alpha$ flare. These time lags yield average velocities as 630, 1370, and 1260 km s^{-1} , respectively.

Several ARs were present on the solar disk during the disk passage of AR MWO 5726, and some of these regions also produced $H\alpha$ flares albeit none of the other ARs produced flares of importance 3 as recorded in the QBSA. For example, on January 14, a relatively large $H\alpha$ flare of importance 2+ was observed at N25W35, close to AR MWO 5719. The ICMEs originating west of central meridian are more likely to be geo-effective as compared with the ICMEs originating east of Sun’s central meridian (Gopalswamy et al. 2007). Thus, the geomagnetic storm on January 17 may be related to an ICME originating from region MWO 5719, not from region MWO 5726. Nevertheless, both eruptions occurred at about the same time, and thus, this difference in the source region is not important for estimating the time between the ICME liftoff and the onset of the geomagnetic storm.

However, the reported flares were probably no more than a part of the entire solar flare activity in this interval. Notably, we have 10 radio fade-outs reported in the Eastern USA (Table 3 of Gilliland et al. 1938) and several solar flare effects (SFEs) in this interval (e.g., Bartels et al. 1939; Yokouchi 1953). Therefore, for the first geomagnetic storm on 17 January, we have two more possible scenarios, as relatively large SFEs (see, e.g., Curto 2020 for a review) were reported at Cheltenham, Tucson, San Juan, and Huancayo at $\approx 17:07$ UT on 1938 January 15 and at Watheroo, Honolulu, and Kakioka at $\approx 00:40$ UT on 1938 January 16 (see, e.g., Figure 2; Bartels et al. 1939; Yokouchi 1953; Cliver & Svalgaard 2004). The latter was especially accompanied with a notable SFE at Apia (56 nT; Wadsworth 1938), which was probably enhanced with equatorial electrojet due to its proximity to the geomagnetic equator (see e.g., Rastogi et al. 1997). These ionospheric disturbances indicate an intense X-ray flare overlooked in the flare patrols at that time (see D’Azambuja 1938, p. 124). In these cases, as the ICME transit times were ≈ 29.5 and ≈ 21.9 hr (for the latter, see also Bartels et al. 1939; Cliver & Svalgaard 2004), their average ICME velocities are estimated $\approx 1400 \text{ km s}^{-1}$ and $\approx 1900 \text{ km s}^{-1}$, respectively. These scenarios will be further analyzed on the basis of the CR variability recorded in the contemporary ICs in Section 5.

3. Geomagnetic Storms

Upon arrival, these ICMEs caused three consecutive intense geomagnetic storms. Usually, the Dst index is used to characterize the storm intensity and time series to follow the development of the ring current. However, the official Dst

²⁰ <https://solarscience.msfc.nasa.gov/greenwch.shtml>

²¹ Kurochkin (1939) mentions an $H\alpha$ eruption in this AR on January 23 at 7:20–7:30 UT although without a reference to this flare’s importance.

²² http://www.kakioka-jma.go.jp/obsdata/Geomagnetic_Events/Events_index.php

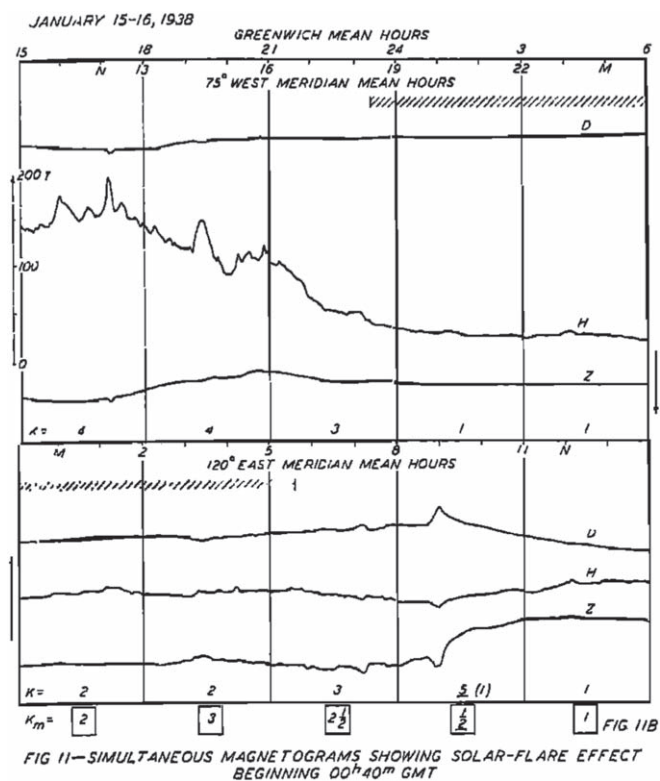


Figure 2. Traces with the SFEs at 17:07 UT on January 15 recorded at Huancayo Observatory (upper panel) and at 00:40 UT on January 16 recorded at Watheroo Observatory (lower panel), adopted from Bartels et al. (1939).

index became available only in 1957 and hence does not cover these storms. Instead, we have used the Dcx index, a so-called corrected and extended version of the Dst index created by the space climate team at the University of Oulu, starting in 1932 (Karinen & Mursula 2005, 2006; Mursula et al. 2008). As Hermanus Observatory started operation only after 1941, the Dcx index in 1938 has been reconstructed with the observations from the neighboring magnetic station of Cape Town as replacement of Hermanus data. We also consulted the hourly data for these four reference stations (Kakioka, Cape Town, San Juan, and Honolulu), and confirmed that they are free from scale-off issues, and cross-checked the calculated results.²³

Figure 3 shows the time series of the hourly Dcx index during 1938 January 14–29. Three major storms were recorded in this interval as identified from the negative excursions with large amplitudes. The first storm peaked at 16 UT on 1938 January 17 with its maximum negative Dcx ≈ -171 nT after its SSC at 22:36 UT on January 16. The second and third storms are often considered as twin storms (see Jones 1955; Lefèvre et al. 2016) and peaked at 11 UT on January 22 with Dcx ≈ -328 nT and 23 UT on January 25 with Dcx ≈ -336 nT.

Jones (1955) identified the geomagnetic storm on 1938 January 25 as among the top 11 storms of the 112 great storms listed between 1874–1954. Of particular note was the apparent “misidentification” of the solar source in the Greenwich Catalog storm tabulation (Jones 1955, pp. 77–81) because of the statistical limits of the distance of Group 12673 from the solar central meridian.

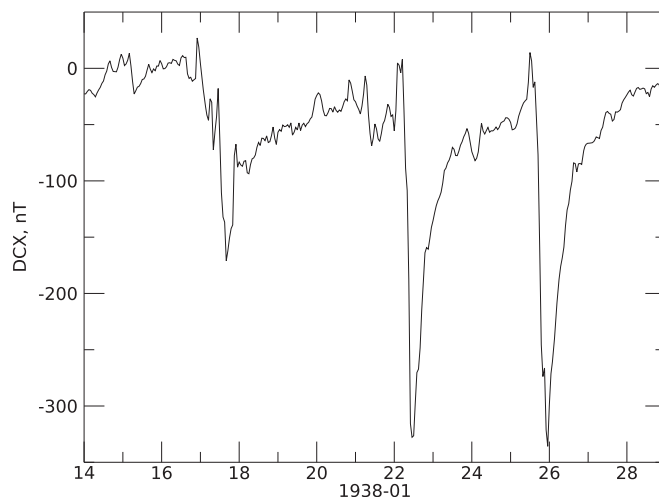


Figure 3. The hourly Dcx index during the period 1938 January 14–29.

The storm intensities of the second and third storms are comparable to the major magnetic storm on 1960 November 12 (Dst = -339 nT) and only slightly weaker than the Halloween storms on 2003 October 29/30 (Dst = -354 nT), and on 2003 October 30/31 (Dst = -383 nT), as well as the extreme storm on 1967 May 25/26 (WDC for Geomagnetism at Kyoto et al. 2015; see also Gopalswamy et al. 2005; Knipp et al. 2016; Lockwood et al. 2019). This amplitude is certainly in an extreme category (Meng et al. 2019), while it does not go beyond the threshold of Dst (or Dst*²⁴ before 1956) being equal to -500 nT (Cliver & Dietrich 2013; Hayakawa et al. 2019, 2020a, 2020b). Caveats must be noted for its uncertainty, as the Dst index and Dcx index are slightly different in the calculation procedure and amplitudes of specific storms in these indices vary up to ≈ 44 nT (see Karinen & Mursula 2006; Mursula et al. 2008; Riley 2017).

4. Low and Midlatitude Aurorae

The auroral oval expands equatorward during major geomagnetic storms (Kamide & Winningham 1977; Yokoyama et al. 1998; Shiokawa et al. 2005). It was also the case during this stormy interval, especially during the storms on January 21/22 and 25/26 (Silverman 2006). In particular the last storm on January 25/26 was characterized by aurorae “seen over practically the whole of Europe, and as far south as Gibraltar and Sicily” (Anon 1938, p. 232).

We have extended investigations on the visual auroral reports across the United States, the USSR, Japan, Australia, and New Zealand, using the summary of auroral observations for the years 1938–1939 published by Kurochkin (1939), the *Climatological Data in the United States* (U. S. Department of Agriculture Weather Bureau 1938), and local reports and newspapers. These reports show that the aurorae extended equatorward for the three storms on 1938 January 17/18, 21/22, and 25/26 (Figure 3). Reports in the United States show the significant latitudinal expansion of auroral visibility during these storms (Figure 4). The *Climatological Data in the United States* reported the auroral visibility during these three geomagnetic storms. Even on January 17/18, the aurorae were visible down to Cheyenne in Wyoming (N41°08′, W104°49′; 50.0° MLAT). The aurorae were predominantly observed in the

²³ <http://wdc.kugi.kyoto-u.ac.jp/caplot/index.html>

²⁴ Here, we denote equivalent Dst estimates with alternative stations as Dst*.

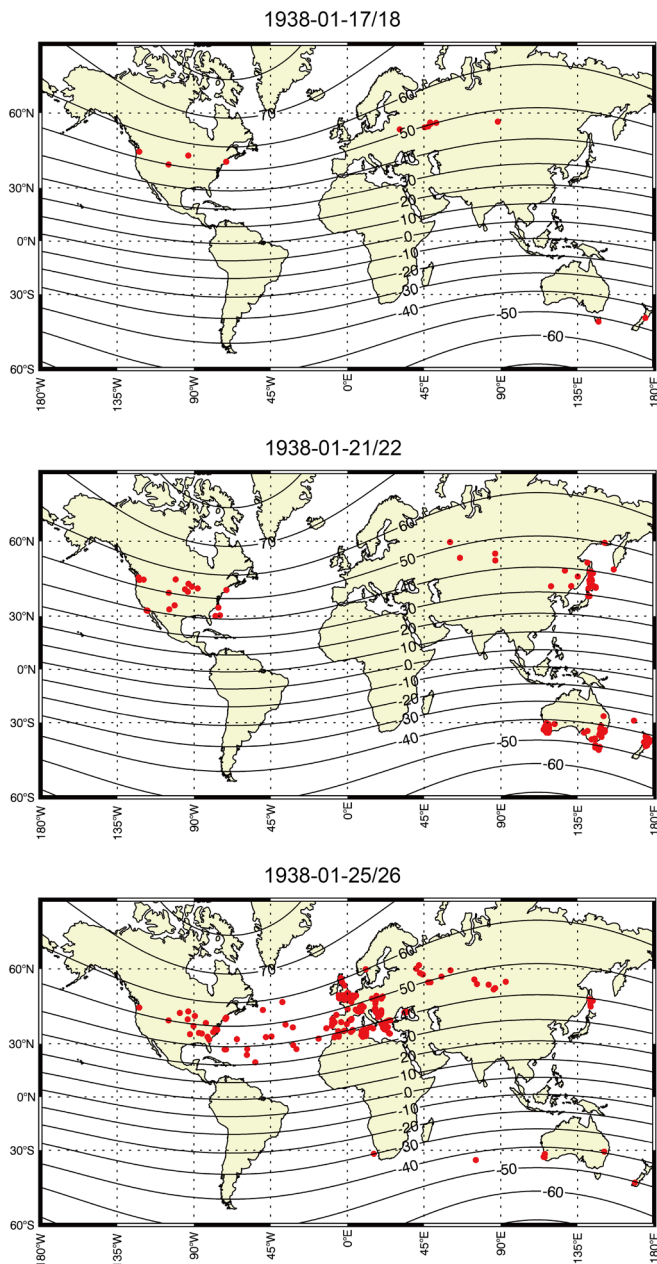


Figure 4. Reported auroral visibility on 17/18 (above), 21/22 (middle), and 25/26 (below) 1938 January (<https://www.kwasan.kyoto-u.ac.jp/~hayakawa/data>). The reports taken at $|\lambda| < 40^\circ$ MLAT have been primarily investigated here and added to the data points in Silverman (2006), on the basis of contemporary reports, such as those in U.S. Department of Agriculture Weather Bureau (1938), the USSR accounts (e.g., Kurochkin 1939), Japanese meteorological reports, and newspapers in Australia and New Zealand. The observational sites are shown with the red dots. The contour lines indicate MLATs with interval of 10° on the basis of the IGRF12 model (Thébault et al. 2015).

central United States on January 21/22 and in the eastern United States on January 25/26.

This was also the case with Australia and New Zealand. The local newspapers show significant auroral visibility on January 17/18, 22/23, and 25/26 (Figure 4). In these countries, the aurorae were most splendid on January 22/23 and visible down to Norfolk Island ($S29^\circ 02'$, $E167^\circ 57'$; -34.9° MLAT). Despite the reduced significance, aurorae were reported during the other nights: down to Wellington ($S41^\circ 17'$, $E174^\circ 46'$; -45.6° MLAT) on January 17/18; and down to Manilla ($S30^\circ 45'$, $E150^\circ 43'$; -39.4° MLAT) on January 25/26.

In the USSR, during January, there were in total 24 auroral nights reported. Five of those auroral displays were so bright that they produced multiple reports from the (geographic) midlatitudes. All aurorae were concurrent with the major geomagnetic storms and were accompanied by interruptions in radio and telegraph communications. Kurochkin (1939) provided a summary of the aurora observations based on the numerous eye-witness letters received by the local newspapers, the Moscow Planetarium, the Division of the Astronomical-Geodetical Society of the USSR, and the Sternberg Astronomical Institute. We supplemented this summary by the additional reports from regional newspapers. The approximate geographic locations of the aurora reports are shown in Figure 4.

Aurora on 1938 January 17 was observed between 13 UT and 22 UT as a diffuse glow near the horizon with pillars growing out of it. The pillars were moving from east to west. The auroral colors in the eastern regions of the USSR were whitish at first, but turned into the reddish hues later. In the western regions, the aurora was mostly red in hue. On January 22, the aurora was first observed in the USSR Far East at a latitude of about 48° . The aurora had a shape of diffuse clouds with the rays of greenish and purple color. The aurora observed in the western part of country was also in the shape of diffuse clouds, but without rays. The auroral features appeared moving from east to west. The strongest auroral activity was observed during January 25–27, and it had been seen as far south as the Crimean Peninsula ($N45^\circ$). On January 25, the aurora was reported as a series of white bands, which later turned into bright-red diffuse clouds. On January 26, in the eastern part of the country, the reports of aurora described it as a series of pillars of red color. In the western regions, the aurora has been seen as a red glow low above the horizon. The brightness of aurora on January 27 was weaker as compared with the previous nights. At the beginning the colors were reported as light red, but gradually changed to a whitish color. The auroral patterns were moving from west to east (Kurochkin 1939). The description of the observed patterns and their colors are in a good agreement with the examples of auroral drawings shown in Figure 5.

Figure 4 shows the geographic distributions of visual auroral reports on 1938 January 17/18, 21/22 and 25/26. As shown here, the auroral visibility actually extended much more equatorward than observed in the European sector. In comparison with Silverman (2006), our investigations show further observations in the northern Japan, including the Southern Sakhalin Island (currently under rule of the Russian Federation) as well as a large longitudinal extension of auroral observations across the former USSR during both of these storms (see, e.g., Figure 4), Northern Australia and Northeastern China (mainly Manchuria at that time) on January 21/22, and Greece and French Northern Africa (modern-time Tunisia, Algeria, and Morocco) on January 25/26. On the basis of the magnetic field model IGRF12 (Thébault et al. 2015), we located the geomagnetic pole at $N78^\circ 29'$, $W068^\circ 27'$ in 1938. Magnetic latitudes (MLATs) of given observational sites were calculated with their angular distance from the geomagnetic pole. Accordingly, the most equatorial auroral visibility was confirmed as 29.5° MLAT at Morioka in Japan ($N39^\circ 42'$, $E141^\circ 09'$; Morioka Observatory 1954, p. 117) on January 21/22 and as -29.9° at the vessel Nardana off South Africa ($S31^\circ 50'$, $E015^\circ 30'$; Anon 1939) on January 25/26. As the geomagnetic dipole strength is continuously declining (e.g., Korte & Constable 2011), these auroral expansions may have



Figure 5. Auroral drawings on 1938 January 22: at Keramui (33.8° MLAT; N43°40', E145°33') at 19:20 LT and 19:25 LT (top and middle; Kisho 1938a) and Paramushir (41.9° MLAT; N50°40', E156°07') at 19:45 LT (bottom; Kisho 1938b). The Keramui drawing at 19:25 LT shows a red background and yellow streaks and mentions perpetual pulsation of the auroral emissions. The Paramushir drawing shows vertical auroral extension. The reddish component and yellow streaks are considered as oxygen emissions at 630.0 nm with some mixture of oxygen emissions at 557.7 nm.

required a slightly stronger solar wind driver than expected from the modern statistics (Siscoe & Christopher 1975; Ebihara & Tanaka 2021).

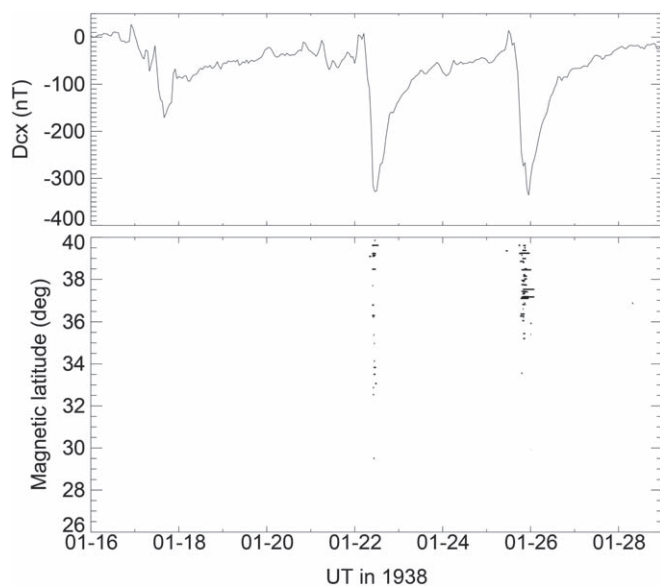


Figure 6. The hourly Dcx index (nT) enlarged from Figure 3 and the low-latitude auroral visibility as a function of $|\lambda|$ and time (<https://www.kwasan.kyoto-u.ac.jp/~hayakawa/data>).

Among these storms, the aurorae on January 21/22 and 25/26 were especially notable in terms of their equatorial extent and were visible even below 40° MLAT. The MLATs of the auroral visibility ($|\lambda| < 40^\circ$ MLAT) are shown in Figure 6 together with the time series of the Dcx index. This figure shows that the aurorae were visible at low latitudes ($|\lambda| < 40^\circ$ MLAT) near the minima of the Dcx index ($Dcx \leq -200$ nT), namely, in the late main phase to the beginning of the recovery phase.

Reports with auroral elevation angle enable us to estimate the equatorial boundary of the auroral oval in combination with their MLATs. Here, we compute the invariant latitude (ILAT) of the footprint of its magnetic field line along which the auroral electrons precipitate (O'Brien et al. 1962; McIlwain 1966), assuming the auroral elevation as ≈ 400 km (Roach et al. 1960; Ebihara et al. 2017). During the storm on January 21/22, the aurorae were reported overhead at Noto in Sakhalin Island (39.2° MLAT; N49°16', E144°00'; Karafuto Department Observatory 1939, p. 6; see Figure 5). Accordingly, its equatorial boundary of the auroral oval is computed as 40.3° ILAT. These results agree with one another and with the report of most equatorial visibility on January 21/22 as well. In this case, the aurorae were probably visible up to $\approx 20^\circ$ in elevation angle at Morioka, at the most equatorial observational site (29.5° MLAT; N39°42', E141°09'; Morioka Observatory 1954, p. 117). On the other hand, during the January 25/26 storm, the aurorae were reported up to 45° in elevation angle at Patras in Greece (37.3° MLAT; N38°15', E021°44'; ΗΔ ΠΑΣΙΣ (I Drasis 1938, p.1). On this basis, its equatorial boundary of the auroral oval has been computed as 40.0° ILAT and compares well with that on January 25/26.

5. Cosmic-Ray Variations

Cosmic-ray (CR) measurements at Earth in 1938 were primarily those from ICs or an occasional balloon flight (Shea & Smart 2000), whereas their calibrations with the neutron-monitor data are still challenging (McCracken 2007; Usoskin et al. 2011; Shea & Smart 2019). Ionization chambers at Cheltenham and Cambridge in the USA, Christchurch in New

Table 1
Locations of the CR Ionization Chambers in 1938 January, Derived from Table 1 of Shea & Smart (2000)

Name ^a	Latitude	Longitude	Altitude (m)	Cutoff Rigidity (GV) ^b
Cambridge, USA (Boston)	N42°22'	W071°05'	3	1.47
Cheltenham, USA	N38°42'	W076°48'	72	2.04
Christchurch, NZ	S43°30'	E172°36'	8	2.82
Hafelekar, Austria	N47°19'	E011°23'	2290	4.26
Teoloyucan, Mexico	N19°12'	W099°12'	2285	10.09
Huancayo, Peru	S12°18'	W075°20'	3350	13.67

Notes.

^a Some researchers refer to these locations by the alternate name given in parenthesis.

^b Vertical cutoff rigidity using the IGRF geomagnetic field coefficients appropriate for 1940.

Zealand, Teoloyucan near Mexico City in Mexico, Huancayo in Peru, and Hafelekar in Austria continuously monitored the CR intensity. In addition to those detectors, the CR group in the Netherlands had an IC onboard a ship with measurements being made at different locations dependent on the route traveled (Shea & Smart 2000).

The availability of CR particles at the top of the atmosphere is dependent on the cutoff rigidity of the detector location. The polar regions are accessible by MeV protons whereas it takes a high-energy particle (≈ 15 GeV) to penetrate the terrestrial magnetic shield to the equatorial atmospheres. The shielded ionization chambers respond primarily to secondary muons generated by the incident particles creating a nuclear cascade in the atmosphere. In order for this short-lived muon²⁵ to survive its transit through the atmosphere to sea level, it must be the product of an incoming nuclei >4 GeV (equivalent to a rigidity of ≈ 4.85 GV). This relativistic energy may be slightly lower for detectors at altitude as the transit path through the atmosphere is slightly shorter.

The detectors at Cambridge, Cheltenham, Christchurch and Hafelekar, with geomagnetic cutoff rigidity values <4.85 GV only detected the muons created by the cosmic radiation above ≈ 4.85 GV. The other two detectors at Teoloyucan and Huancayo only detected the muons created by CRs above their respective cutoff rigidity (See Table 1).

The published traces of CR data (Forbush 1938; Hess et al. 1938) show Forbush decreases during the geomagnetic storms on January 17/18, 21/22, and 25/26. Figure 7 presents the CR intensity as recorded by the Cheltenham and Huancayo ICs during January 13–28. The largest decrease was on January 17/18 with more moderate decreases later in the month. This implies that the magnetic structure(s) responsible for the first geomagnetic storm provided a stronger barrier to CRs than the later magnetic clouds. The double dip in the Dcx index (Figure 6) associated with the first storm on January 16 and 17 is consistent with a strong shock passage, followed by an ICME with a trailing southward field. A modern, but slower,

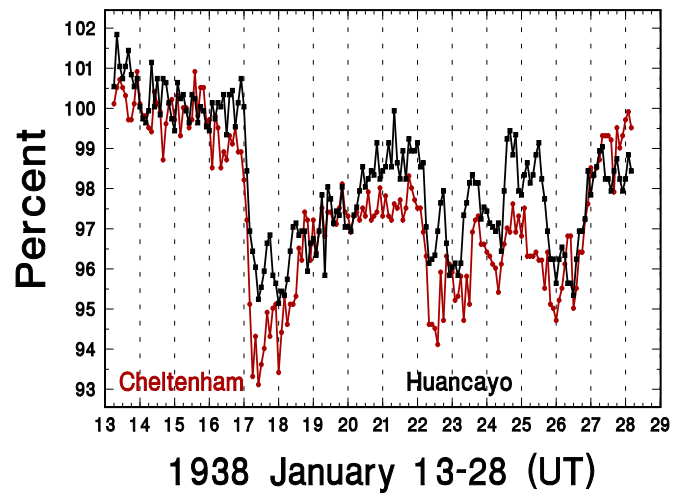


Figure 7. Bi-hourly variability of the CR intensities recorded in the ICs at Cheltenham and Huancayo during 1938 January 13–28, derived from Lange & Forbush (1948). Both LT and UT times are given as the photographic records, the tables in Lange & Forbush (1948) and some of the figures in the publications of Forbush are in LT. Note that the CR intensity shown in Figure 2 of Forbush (1938) is an average of the intensities measured at Boston (i.e., Cambridge), Cheltenham, and Huancayo.

analog for this event can be found in the shock/ICME passage of 2000 October 12–14 (see Figure 3 of Richardson & Cane 2010) and associated indices in the OMNIWeb database. Furthermore, we suggest that the orientation of the ICME upon arrival at the Earth's magnetosphere was such that the southward component of the interplanetary magnetic field had a moderate magnitude, thus giving rise to a more moderate storm than the following ICMEs.

The geomagnetic storm on January 17/18 had two possible solar origins: from either the solar activity 04:40–05:30 UT on January 14 ($H\alpha$ patrol) or 00:40 UT on January 16 with an SFE. The latter event with a fast ICME (average velocity 1900 km s^{-1}) seems the most likely progenitor of the SSC at Earth at 22:36 UT and the resulting Forbush decrease. This is because the large AR MWO 5726 was located around N18W30 at the time of the SFE (essentially the X-ray flare; see Figures 1 and 2) based on the Greenwich Photoheliographic Records and was more favorably located for a fast CME to travel to Earth producing the largest Forbush decrease of this series of events.

The possibility of a solar proton event during this active period has been considered (e.g., Besprozvannaya 1962). Interestingly, almost simultaneously, a complete blackout of shortwave communications was reported in the polar region during 1938 January 16–19 (Moisejev 1939b). Švestka (1966) citing Besprozvannaya (1962) includes 1938 January 16 among his list of polar blackout events, but Švestka did not include this event in his list of possible proton events. Besprozvannaya (1962) listed indirect data for an abnormal polar cap absorption on January 16, but no time was given. Besprozvannaya's data were from vertical incidence ionospheric soundings from Tikhaya Bay (N80°19', E052°47'). At 00:40 UT on 1938 January 16, the time of the SFE, Tikhaya Bay was under polar night. An SFE is indicative of a strong X-ray event, and while there is no solar activity listed in the QBSA (D'Azambuja 1938), it is possible there were no solar optical observations at that time. A large solar X-ray event at 00:40 UT would not have impacted the ionosphere above Tikhaya Bay; however, a solar proton event with particles >10 MeV could easily

²⁵ The half life of a muon in the laboratory frame is 2.2 μs .

The percentage increase in ionization current in the Cheltenham ionization chamber

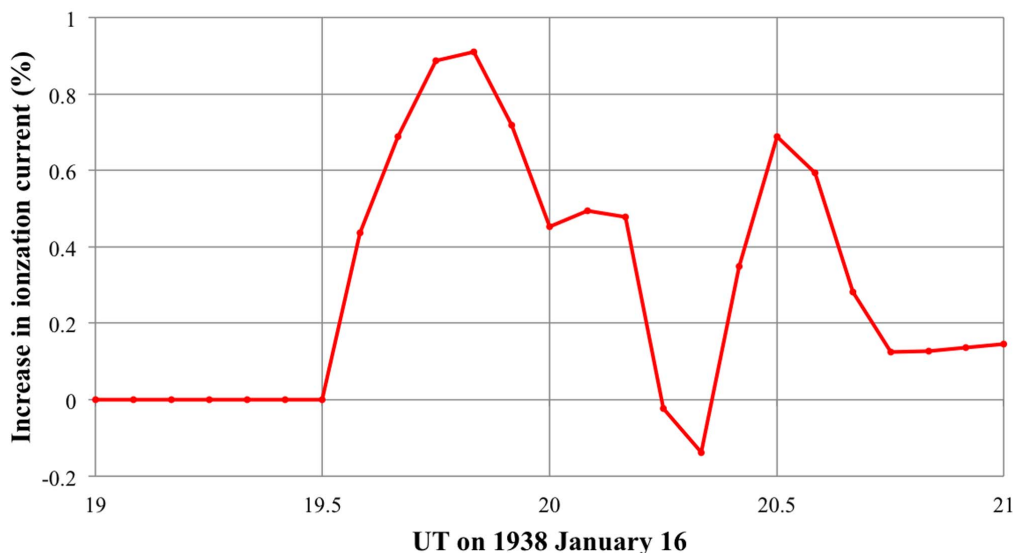


Figure 8. The percentage increase in ionization current in the Cheltenham IC, derived from the digital copies of the original real-time photographic records from the Carnegie ICs preserved at the National Centers for Environmental Information.

produce a polar cap blackout in the dark polar regions as determined by simultaneous measurements of solar proton events and polar cap riometer absorption (Sellers et al. 1977; see also Shea & Smart 2012).

Scanned copies of the original real-time photographic records from the Carnegie ICs are available at the National Centers for Environmental Information, Data Services Division, Asheville, North Carolina, in the USA. The Carnegie ICs have been described previously (Compton et al. 1934). A brief summary is appropriate here to better understand a unique characteristic of these detectors: their high temporal resolution. The IC was an analog instrument with an intrinsic time constant <1 minute, and the time integral of the ionization current was recorded on a moving photographic strip with a temporal resolution of better than 1 minute.²⁶ Consequently, these detectors provided a detailed minute-by-minute record of the intensity of the cosmic radiation. Normally the trace rose or fell at a smooth essentially monotonic rate within the hour, except when a ground-level enhancement (GLE) was detected immediately displaying an abrupt and subsequently strongly variable change in the slope of the trace. One of the authors of this article (KGMcC) built and operated an IC and has examined at least 30,000 hourly traces over his career, including all the known GLEs between 1940–1960 as recorded by the Carnegie ICs. In all those 30,000 records, there were no sharply variable traces other than the known GLEs in 1942, 1946, 1949, 1956, and 1960.

We have scanned the IC records from both the Cheltenham and Christchurch detectors for 1938 January and several subsequent months. During 1938 January, both ICs exhibited the relatively slow hour-by-hour variations including the Forbush decreases shown in Figure 8. The standard deviation of an hourly increase in ionization current was estimated to be 1.0% in Tatel’s Carnegie Institute Workbook. At $19:35 \pm 2$ UT the Cheltenham ionization

current increased sharply within one minute varying thereafter as shown in Figure 8. Following a broad 30 minute maximum, it had disappeared by 22:00 UT. Close inspection of the photographic records shows a double pulse: the onset of the first increase at $\approx 19:35$ UT (14:35 LT) and the second one at $\approx 20:25$ UT (15:25 LT). Integrated over the period 19:35–22:00 UT the enhancement represents an increase in CR intensity of less than one standard deviation and could not be classed as a GLE only on that basis. However our interpreters’ experience with this now rare type of recording; the complete absence of any other similar sharp changes in 30,000 hourly records other than in GLE; and its strong similarity to the sharp temporal variations during known GLE leads us to record the possibility that it may be such in the analysis of this unusual series of solar events. This possibility is strengthened by the ionospheric and radio observations outlined below. We note, however that the Christchurch IC trace looked normal with little recognizable deviations from the norm. Therefore, there was no evidence of a correlating enhancement at Christchurch in the Southern Hemisphere at a similar geomagnetic cutoff to Cheltenham in the Northern Hemisphere, indicative of an anisotropy as is common in GLE.

A small enhancement of the type shown in Figure 8 would not have been considered significant by Dr. Forbush whose main interest at that time was in geomagnetic field variations and whose supervisor was adamant that the Sun could not accelerate CRs to relativistic energies (S. Forbush’s personal communication with KGMcC in 1962). The concept of a solar CR event did not occur until the large events in 1942, but it was not until 1946 when these data and their interpretation were published (Forbush 1946).

An example of a small muon increase associated with a significant GLE was recorded during the complex array of multiple CMEs and interplanetary shocks in 1960 November. For the GLE on 1960 November 12, the high sensitivity MIT muon detector only recorded a 1% increase compared to $\approx 60\%$ for several neutron monitors (Steljes et al. 1961). That GLE and the following one (1960 November 15) were not

²⁶ See Figure 6.2–1 of Beer et al. (2012) for an example of a GLE as recorded by the Christchurch IC on 1942 March 7.

discernible in the Cheltenham (Fredrichsburg) IC record. That is, on the basis of the evidence from muon detectors, the putative event on 1938 January 16 (Figure 8) was possibly more intense than the well-documented, substantial, and initial anisotropic GLE on 1960 November 12. While further evidence is needed to prove the small increase at Cheltenham between $\approx 19:35$ and $20:45$ UT on 1938 January 16 as a GLE, we note the following:

(1) Radio fade-outs occurred in the Eastern USA from 16:40–20:20 UT on January 16 (Gilliland et al. 1938).

(2) Approximately 18 hr after the Cheltenham increase, the disturbances in the geomagnetic field greatly intensified indicative of the possible arrival of yet another interplanetary shock during this highly disturbed period. There was also an additional short decrease in the galactic CR intensity that had just started to recover from the previous geomagnetic storm (see Figures 3 and 7).

This sequence seems more than just a coincidence. We can infer from all of the flare activity during January 14–16 that there were likely multiple ICMEs, possibly interacting and merging on their way to Earth. The reported radio fade-outs between Ohio and Washington, DC from 16:40–20:20 (Gilliland et al. 1938) imply their cause as a long duration X-ray event, or an influx of GeV protons, or their combination. This strongly suggests significant solar activity between $\approx 16:40$ – $20:20$ on January 16. In order to reach the path between Ohio and Washington ($\approx 50^\circ$ – 55° MLAT, see Figure 4), the protons would have to have a rigidity in excess of 2 GV thus lending credit to a hypothesized high-energy particle event.

To summarize the sequence of activity, we know that an ICME was advancing close to Earth as evidenced by an SSC at 22:36 UT on January 16. If another flare occurred around 19:35 UT with the acceleration of high-energy (GeV) protons, those protons would pass through the intervening shock front to arrive at Earth. The slightly less energetic particles, moving slower, would most likely be accelerated by the magnetic fields in the shock front of both the secondary ICME and the primary ICME. Such particles might have been trapped/scattered between the preceding merged interaction region and the new advancing ICME as in the 1972 August sequence (e.g., Knipp et al. 2018).

We thus assess the enhancement at 19:35 UT on 1938 January 16 as a plausible—but not yet confirmed—GLE before the earliest known GLE reported on 1942 February 28 (Forbush 1946), on the basis of consistent overall enhancement in the scaled data at Cheltenham. This finding may let us chronologically bridge the known GLEs (McCracken 2007; Shea & Smart 2019; Usoskin et al. 2020b) and historical GLEs in 774/775 and 993/994 confirmed in the tree rings and ice cores (Miyake et al. 2012, 2013; Usoskin et al. 2013; Mekhaldi et al. 2015), which is considered a factor of 50–100 stronger than the strongest known GLE of 1956 February 23 (e.g., Mekhaldi et al. 2015; Miyake et al. 2019; Cliver et al. 2020; Usoskin et al. 2020a). Moreover, this extended timescale is typical of a GLE originating from solar activity near and east of the solar central meridian (McCracken & Palmeira 1960; Stoker 1995, p. 362). The GLE on 1981 October 12, associated with solar activity at E31, had an initial onset at 06:45 UT recorded by the Goose Bay neutron monitor in Canada and a broad maximum intensity of 8.5% between 08:45 and 10:00 UT as shown in the GLE database at

Oulu University²⁷ (Poluianov et al. 2017; Gil et al. 2018; Usoskin et al. 2020b; D. F. Smart 2020, private communication). This interpretation is consistent with the location of the flare-productive AR (MWO 5726) in the eastern solar disk at that time (Figure 1). Thus, there are two possible source flares for a possible solar proton event on 1938 January 16: the SFE at 00:40 UT or unreported solar activity around 19:35 UT.

6. Discussion

Our study confirms the arrivals to Earth of three ICMEs in late 1938 January, as implied by the occurrence of intense geomagnetic storms and Forbush decreases (summarized in Table 2). The Sun was extremely active in this interval, probably because of hyper-productive ARs such as AR 5726 (RGO 12673). With a significant level of sunspot and flare activity during January 14–22, the source region of the ICME associated with the geomagnetic storm on January 17/18 is somewhat uncertain, hosting the two major H α flares at 04:40–05:30 on January 14 (from AR 5726 at N10E45 and AR 5719 at N25W35) and two large SFEs at 17:07 on January 15 and at 00:40 on January 16 as its possible sources. The largest Forbush decrease ($\approx 6\%$) as recorded by ICs on January 17/18 in this sequence indicates its source to be from a fast ICME originating from somewhere near the disk center. Therefore, based on the relative proximity of the source AR from the disk center in calculation (N17E31), we consider the SFE at 00:40 on January 16 as its probable source.

If this was the case, the initial ICME was the fastest with its average velocity of ≈ 1900 km s⁻¹, in contrast with the second and third ICMEs (≈ 1370 km s⁻¹ and ≈ 1260 km s⁻¹, respectively). The amplitudes of the corresponding SSCs at the Kakioka Observatory were unusual in terms of occurrence frequency on the basis of its regular observations in 1924–2013 (Figure 4 of Araki 2014). As the SSC amplitude (ΔH) is empirically described as $\Delta H = C\Delta P^{1/2}$, where $C = 15$ nT/nPa^{1/2} and ΔP means change in the solar wind dynamic pressure (Araki 2014; see also Siscoe et al. 1968), the ΔP for each of these ICMEs is computed as ≈ 23 , ≈ 18 , and ≈ 18 nPa, respectively. The estimated dynamic pressures are much higher than those for the more common ICMEs and are therefore classified as extreme cases (e.g., Lugaz et al. 2015). The lower limit of the solar wind density can be estimated by the equation $n = \Delta P/mV^2$, where m means the solar wind mass (≈ 1.16 times proton mass), n means the solar wind density, and V means solar wind velocity (Araki 2014). On this basis, the lower limit of the solar wind density of these ICMEs is roughly estimated ≈ 3 cm⁻³, ≈ 5 cm⁻³, and ≈ 6 cm⁻³, respectively. Additionally, the dynamic pressures of the solar wind before the shock arrivals are unknown, and they probably make the actual solar wind density slightly higher than our estimate.

For the first storm, the SSC amplitude is greatest, and the magnitude of Forbush decrease is the maximum (Table 1). We consider that the initial ICME was the strongest in terms of speed and dynamic pressure of the solar wind as well as the magnitude of the IMF in comparison with the second and third ICMEs. Nevertheless, the magnitude of the first geomagnetic storm was weaker ($D_{cx} \approx -171$ nT) in comparison with the other two (≈ -328 nT and ≈ -336 nT), unlike the magnitudes of the Forbush decreases for these ICMEs ($\approx 6\%$ versus $\approx 3\%$ and $\approx 2\%$). This contrast can be explained by the weaker southward

²⁷ <https://gle oulu.fi>

Table 2

Time Series for the Major Solar Flares, SSCs, Forbush Decreases, and Geomagnetic Storms in the Interval of 1938 January 14–26, Examined in this Article

Date	Time (UT)	Event	Magnitude	Reference	Notes
14	0440–0530	Flare	3	D’Azambuja (1938)	AR 5726 at N10E45
14	0440–0530	Flare	2+	D’Azambuja (1938)	AR 5719 at N25W35
14	1629–1835	RF	...	Gilliland et al. (1938)	In the Eastern USA
14	1840–1857	RF	...	Gilliland et al. (1938)	In the Eastern USA
15	1707	SFE	...	Bartels et al. (1939)	At Huancayo, etc.
15	1708–1724	RF	...	Gilliland et al. (1938)	In the Eastern USA
15	1719–1737	Flare	2	D’Azambuja 1938	AR 5719 at N21W53
15	1838–1935	RF	...	Gilliland et al. (1938)	In the Eastern USA
16	0040	SFE	...	Bartels et al. (1939)	At Watheroo
16	0045–0300	SFE	...	Yokouchi (1953)	At Kakioka
16	0044	SFE	...	Wadsworth (1938)	At Apia
16	...	PCA	...	Besprozvannaya (1962)	Indirect data
16	1640–2020+	RF	...	Gilliland et al. (1938)	In the Eastern USA
16	≈1900	RF	...	Spokane Daily Chr., 1938 January 17	In the Western USA
16	1935–2025	GLE?	...	Cheltenham IC	A plausible GLE
16	2236	SSC	72 nT	Kakioka ED	...
17	≈16	GMS	−171 nT	Dcx index	...
17	...	FD	≈6%	Forbush (1938)	...
19	1115–1200	Flare	2	D’Azambuja (1938)	AR 5726 at N15W25
19	2238–2312	RF	...	Gilliland et al. (1938)	in the Eastern USA
20	1608–1800	Flare	2	D’Azambuja (1938)	AR 5726 at N24W23
20	1820–2127	Flare	3	D’Azambuja (1938)	AR 5726 at N18W30
20	1800–1840	RF	...	Gilliland et al. (1938)	In the Eastern USA
20	1902–2040	RF	...	Gilliland et al. (1938)	In the Eastern USA
21	1640–1920	RF	...	Gilliland et al. (1938)	In the Eastern USA
22	0242	SSC	63 nT	Kakioka ED	...
22	...	GMS	−328 nT	Dcx index	...
22	...	FD	≈3%	Forbush (1938)	...
24	0100–0130	Flare	2	D’Azambuja (1938)	AR 5726 at N22W85
24	0300–0340	Flare	3	D’Azambuja (1938)	AR 5726 at N22W85
24	0512–0700	Flare	3	D’Azambuja (1938)	AR 5726 at N22W80
24	1810–1850	RF	...	Gilliland et al. (1938)	In the Eastern USA
25	1151	SSC	63 nT	Kakioka ED	...
25	≈23	GMS	−336 nT	Dcx index	...
25	...	FD	≈2%	Forbush (1938)	...

Note. Here, we have used abbreviations of SFE (solar flare effect), PCA (polar cap absorption), GLE (ground-level enhancement), SSC (storm sudden commencement), GMS (geomagnetic storm), FD (Forbush decrease), RF (radio fade-out), and Kakioka ED (Kakioka Event Database).

component of the IMF in the initial ICME. It should be also noted that their variable impact angles might have played another role. The solar wind density sometimes contributes to the intensification

of the ring current, in addition to the solar wind speed and the southward component of the IMF (Thomsen et al. 1998; Smith et al. 1999; Ebihara & Ejiri 2000; O’Brien & McPherron 2000).

However, the intensity of the ring current is suggested to be disproportional to the solar wind density because of the shielding electric field that impedes the intensification of the ring current (Ebihara et al. 2005).

On the basis of the sunspot positions (N17E31, N18W30, N22W85, and N22W80), it is also speculated that only part of the ICMEs impacted the terrestrial magnetosphere upon the first and third SSCs (see Cliver 2006; Gopalswamy et al. 2005, 2007). The first ICME had at least three scenarios and the ICMEs of initial two eruptions (at 04:40–05:30 on January 14 and 17:07 on January 15) may have cleared the path for the ICME of the third eruption (at 00:40 on January 16). Similar cases are found in the Hydroquebec storm in 1989 March and the Halloween sequence in 2003 October. Around the Hydroquebec storm on 1989 March 13/14, AR 5395, a large and complex δ -type sunspot group, caused a sequence of flares including 11 X-class flares such as the March 6 flare (X15) and March 17 flare (X6.5) (Allen et al. 1989; Boteler 2019). Similarly, AR 10486 caused a series of flares and launched a series of ICMEs, which resulted in major geomagnetic storms of the Halloween storm category (Gopalswamy et al. 2005, 2007; Lefèvre et al. 2016; Shiota & Kataoka 2016).

This stormy sequence caused a series of space weather hazards in 1938 January (e.g., Lennahan 1938). As described above, the USSR polar region witnessed a complete blackout of shortwave communications on 1938 January 16–19. In the American sector, the *New York Herald Tribune* (1938 January 26, p. 21) and the *Phoenix Arizona Republic* (1938 January 26, p. 1) reported radio disruptions even troubling airline flight operations on Monday (January 17), Friday (January 21), and the date immediately before the release of the article (January 25). During and after the sudden storm commencement on January 16, Western Union Telegraph Company and American Telephone and Telegraph each reported strong effects of geomagnetically induced currents in the eastern portion of the USA (The Christian Science 1938). Western Union Telegraph Company reported slight effects of geomagnetically induced currents beginning on January 22 as well. The problems increased in intensity until the afternoon of January 25, when maximum readings exceeding 400 V were recorded in many parts of the United States (Willever 1938). Dr. Dinsmore at Griffith Observatory reportedly saw “one large gas eruption or prominence” in connection with the great sunspot on Monday (January 24). Dr. Frederick Seares of the Mount Wilson Observatory noted, “The radio fade-outs are caused by energy, which comes from one of the gas eruptions to Earth with the speed of light.” This could be associated with the limb eruption of the ICME around the fourth flare on the same date (January 24). With caveats on the chronological uncertainty, the flare reported in Australia, the erupting prominence, the geomagnetic storms, and the radio blackouts affecting airlines are all connected. Radio disruptions can be from flares, radio bursts, or CME-driven geomagnetic/ionospheric storms as shown for the 1967 May storm (Knipp et al. 2016). As such, these reports in the *Tribune* and *Arizona Republic* show early parallels to the 1967 May storm, appearing in the 1938 January literature, however, apparently less dramatically.

7. Conclusions

In this article, we have evaluated the time series and intensities of the solar-terrestrial storms in 1938 January. These major storms occurred around the maximum of Solar Cycle 17,

quite consistently with the existing statistics of occurrence frequency of such space weather events (Lefèvre et al. 2016). Here, we have located four major flares with importance of “3” in $H\alpha$ flaring area on 14 (04:40–05:30 UT), 20 (18:20–21:27 UT), and 22 (03:00–03:40 UT and 05:12–07:00 UT) January, from a giant AR of RGO 12673 (=3627 msh). We also identified a large SFE at 00:40 UT on January 16, which was presumably launched from the same AR.

These flares were followed by three major storms and therefore indicate at least three major ICMEs in this interval. Three SSCs show their arrival time on January 16 (22:36 UT, 72 nT), 22 (02:42 UT, 63 nT), and 25 (11:51 UT, 63 nT), as observed at the Kakioka Observatory. Taking the time of flare as the CME eruption and the time of the SSCs as the time of arrival at Earth, we have evaluated the parameters of these ICMEs: their average velocity as $\approx 1900 \text{ km s}^{-1}$ (first ICME), 1370 km s^{-1} (second ICME), and 1260 km s^{-1} (third ICME); their solar wind dynamic pressure as ≈ 23 , ≈ 18 , and $\approx 18 \text{ nPa}$; and lower limit of their solar wind density as $\approx 3 \text{ cm}^{-3}$, $\approx 5 \text{ cm}^{-3}$, and $\approx 6 \text{ cm}^{-3}$, respectively. Our estimates classify these ICMEs into the extreme category (e.g., Lugaz et al. 2015).

The intensity and evolution of these three major storms have been evaluated with the D_{cx} index, which was calculated on the basis of midlatitude magnetograms. The storm intensities and their peaks have been estimated as $D_{cx} \approx -171 \text{ nT}$ at 16 UT on January 17, $D_{cx} \approx -328 \text{ nT}$ at 11 UT on January 22, and $D_{cx} \approx -336 \text{ nT}$ at 23 UT on January 25. Accordingly, it is shown that two major storms, which are almost comparable to each other, followed a less intense storm.

During the storms on January 21/22 and 25/26, great auroral displays were globally reported. Investigating aurorae visible at low latitudes ($|\lambda| < 40^\circ$), we have located the equatorial boundary of the auroral visibility down to 29.5° MLAT and 29.9° MLAT during these two storms on January 21/22 and 25/26. On the basis of the records with an elevation angle, we have also reconstructed the equatorial boundaries of the auroral oval for these storms as $\approx 40^\circ$ ILAT for each. This also shows that these two storms rivaled each other unlike what has been discussed so far (Silverman 2006) and enhance the role of the January 21/22 storm more than has been previously considered.

Comparing the time series of the magnetic disturbance and the visibility of the low-latitude aurorae, we have revealed that low-latitude aurorae ($|\lambda| < 40^\circ$) were reported around the peak of the geomagnetic storms ($D_{cx} \leq -200 \text{ nT}$). The aurorae on January 21/22 were most seen around Japan as it peaked at 11 UT (late evening in the Japanese sector). On the other hand, the aurorae on January 25/26 were most seen around the Mediterranean Sea, as it peaked at 23 UT (close to midnight in the European sector).

In combination with the first less intense storm on January 17/18, it is suggested that the first massive and fast ICME swept the interplanetary space, allowing the following two more major ICMEs to be much more geo-effective despite their relatively more moderate dynamic pressure. These cases show that a sequence of ICMEs makes its consequences much more serious to the modern technological infrastructure than a single major ICME or a resultant geomagnetic storm. Our results show that a “perfect storm” was formed in 1938 mid-January, just like a sequence of the major geomagnetic storms associated with the so-called “Halloween storm” in 2003 October and other perfect storms in 2017 July, 2012 July, and 1972 August, where large sunspot ARs are capable of launching multiple ICMEs in rapid

sequences (Cliver & Svalgaard 2004; Gopalswamy et al. 2005; Knipp et al. 2018; Liu et al. 2019).

The contemporary IC measurements of the CR intensity have recorded three major Forbush decreases upon the arrival of these three ICMEs. These data show that the initial decrease was the largest ($\approx 6\%$) in accordance with their SSC amplitudes and in contrast with their Dcx intensities. The amplitude of CR decrease depends on the ICME magnetic field and speed (Richardson et al. 1996; Bhaskar et al. 2016). The stronger the magnetic field and speed of the ICME, the larger the CR decrease. This indicates the initial geomagnetic storm was likely caused by a faster ICME than the following ICMEs and makes the SFE at 00:40 UT on January 16 its probable source. Contemporary records of the polar cap absorption indicate the occurrence of a significant solar proton event on January 16. This could be associated with the SFE at 00:40 UT on this date. Otherwise, close inspection of the original traces of the Cheltenham IC measurements reveals a small double pulse at $\approx 19:35$ UT and $\approx 20:25$ UT, indicating the potential occurrence of a weak GLE on this date, thus predating the earliest known GLE in the observational history. This plausible—but not yet confirmed—GLE may also be the source for the polar cap absorption.









This work was supported in part by grant No. 19-02-00088 by RFBR, projects HISTIGUC (PTDC\FER-HFC\30666\2017), MAG-GIC (PTDC/CTA-GEO/31744/2017), JSPS Grants-in-Aid JP15H05812, JP17J06954, JP18H01254, JP20K22367, JP20K20918, and JP20H05643, JSPS Overseas Challenge Program for Young Researchers, the 2020 YLC collaborating research fund, and the research grants for Mission Research on Sustainable Humanosphere from Research Institute for Sustainable Humanosphere (RISH) of Kyoto University, Young Leader Cultivation (YLC) program of Nagoya University, and Comprehensive Research on the Slavic Eurasian Region in Fiscal Year 2021 of the Slavic-Eurasian Research Center (Hokkaido University). We thank Afroditi Nasi, Varvara Kotsiourou, and Kosuke Fukuda for helping us interpreting the contemporary Greek newspapers; and Chiaki Kuroyanagi for helping us interpreting the contemporary USSR and Eastern European newspapers. We thank Don F. Smart for important advice and discussions on interpretations of the IC data. We thank Murray Parkinson, Helen Fischeler, John Kennewell, Michael Wheatland, and Donald Melrose for their helpful advice on the Australian flare patrol records. We thank Roger Ulrich for his helpful advice on the MWO flare patrol records. We thank Ian Richardson for his helpful discussions on Dst profiles for the shock of ICMEs. We thank Mount Wilson Observatory and Meudon Observatory for providing copies of sunspot drawings and spectroheliograms at that time. H.H. thanks Ilya G. Usoskin for his helpful comments on the early CR reports, Sam M. Silverman for his helpful advice on the auroral sightings in the West Europe and North America, José R. Ribeiro and Ana Correia for their helpful discussions on the Iberian auroral sightings, Aki Machida and Koji Mikami for their advice on the archival materials in the Japan Meteorological Agency, and Denny M. Oliveira and Sean P. Blake for their helpful discussions on the ICMEs. HH also thanks Solar Science Observatory of the NAOJ for providing copies of the *Quarterly Bulletin on Solar Activity* and Shingo Nagamachi for his advice on the observational data at the Kakioka Observatory. H.H. has benefited from discussions within the ISSI International Team #510 (SEESUP Solar Extreme Events: Setting Up a Paradigm) and ISWAT-COSPAR S1-02 team. A.A.P. thanks the GOOGLE

Books Team for promptly reviewing the request and releasing the electronic version of the Bulletin of the Astronomical-Geodetical Society of the USSR, Issues 1–4. A.A.P. is a member of the international team of Modeling Space Weather and Total Solar Irradiance over the Past Century supported by the International Space Science Institute (ISSI), Bern, Switzerland and ISSI-Beijing, PRC. D.J.K. was partially supported by AFOSR grant No: FA9550-17-1-0258. CITEUC is funded by Portuguese Funds through FCT (project: UID/MULTI/00611/2019) and FEDER through COMPETE 2020 Operational Programme Competitiveness and Internationalization (project: POCI-01-0145-FEDER-006922).

Data Availability

The SSCs and geomagnetic storms recorded at the Kakioka Observatory were acquired from the Kakioka Event Database. The results presented in this paper (Figure 3) use Dcx indices provided by the Dcx server of the University of Oulu, Finland (<http://dcx.oulu.fi>). Figure 1 is a composite using modified drawings from Mount Wilson Observatory and a spectroheliogram from Meudon Observatory. The auroral data in this article has been summarized in <https://www.kwasan.kyoto-u.ac.jp/~hayakawa/data>. The hourly magnetic measurements and the standard Dst index have been acquired from the WDC for geomagnetism at Kyoto. The international sunspot number has been provided from WDC SILSO (Sunspot Index and Long-term Solar Observations). The newspapers in Australia and New Zealand are consulted in the collections of the National Libraries of Australia and New Zealand. We thank Shawn Hardy of the Carnegie Institute for carefully preserving the original Forbush IC records, the National Geophysical Data Center in Boulder, Colorado, for digitizing many of the original records, and the National Centers for Environmental Information, Data Services Division, Ashville, North Carolina, for archiving these original records. The modern GLE data captured in the neutron monitors have been acquired from the GLE Database of the University of Oulu (<https://gle.oulu.fi>).

ORCID iDs

Hisashi Hayakawa  <https://orcid.org/0000-0001-5370-3365>
 Kentaro Hattori  <https://orcid.org/0000-0001-9933-0023>
 Alexei A. Pevtsov  <https://orcid.org/0000-0003-0489-0920>
 Yusuke Ebihara  <https://orcid.org/0000-0002-2293-1557>
 Ken G. McCracken  <https://orcid.org/0000-0002-0446-3585>
 Ioannis A. Daglis  <https://orcid.org/0000-0002-0764-3442>
 Ankush T. Bhaskar  <https://orcid.org/0000-0003-4281-1744>
 Paulo Ribeiro  <https://orcid.org/0000-0002-4430-7149>
 Delores J. Knipp  <https://orcid.org/0000-0002-2047-5754>

References

- Allen, J., Frank, L., Sauer, H., & Reiff, P. 1989, *EOSTr*, 70, 1479
 Anon 1938, *Natur*, 141, 232
 Anon 1939, *Marine Observer*, 16, 11
 Araki, T. 2014, *EP&S*, 66, 164
 Baker, D. N., Balstad, R., Bodeau, J. M., et al. 2008, *Severe Space Weather Events—Understanding Societal and Economic Impacts* (Washington, DC: National Academies Press)
 Bartels, J., Heck, N. H., & Johnston, H. F. 1939, *TeMAE*, 44, 411
 Bhaskar, A., Vichare, G., Arumbabu, K. P., & Raghav, A. 2016, *Ap&SS*, 361, 242
 Becker, U. 1955, *ZA*, 37, 47
 Beer, J., McCracken, K., & von Steiger, R. 2012, *Cosmogenic Radionuclides* (Heidelberg: Springer)

- Berdugina, S. V., & Usoskin, I. G. 2003, *A&A*, **405**, 1121
- Besprozvannaya, A. S. 1962, *JPSJS*, **17**, 146
- Boteler, D. H. 2019, *SpWea*, **17**, 1427
- Brueckner, G. E., Howard, R. A., Koomen, M. J., et al. 1995, *SoPh*, **162**, 357
- Bumba, V., & Howard, R. 1965, *ApJ*, **141**, 1502
- Carapiperis, L. N. 1956, *GeoPA*, **35**, 139
- Cid, C., Palacios, J., Saiz, E., Guerrero, A., & Cerrato, Y. 2014, *JSWSC*, **4**, A28
- Clette, F., & Lefèvre, L. 2016, *SoPh*, **291**, 2629
- Cliver, E. W. 2006, *AdSpR*, **38**, 119
- Cliver, E. W., & Dietrich, W. F. 2013, *JSWSC*, **3**, A31
- Cliver, E. W., Hayakawa, H., Love, J. J., & Neidig, D. 2020, *ApJ*, **903**, 41
- Cliver, E. W., & Svalgaard, L. 2004, *SoPh*, **224**, 407
- Compton, A. H., Wollan, E. O., & Bennett, R. D. 1934, *RSci*, **5**, 415
- Correia, A. P. S., & Ribeiro, J. R. 1996, *Farol de Esposende*, **10**, 1996-09-05, [in Portuguese]
- Curto, J. J. 2020, *JSWSC*, **10**, 27
- D'Azambuja, L. 1938, *QBSA*, **41**, 123
- Daglis, I. A. ed (ed.) 2001, *Space Storms and Space Weather Hazards* (Berlin: Springer)
- Daglis, I. A. ed (ed.) 2005, *Effects of Space Weather on Technology Infrastructure* (Berlin: Springer),
- Daglis, I. A. 2006, *SSRv*, **124**, 183
- Daglis, I. A., Thorne, R. M., Baumjohann, W., & Orsini, S. 1999, *RvGeo*, **37**, 407
- Domingo, V., Fleck, B., & Poland, A. I. 1995, *SoPh*, **162**, 1
- Ebihara, Y., & Ejiri, M. 2000, *JGR*, **105**, 15843
- Ebihara, Y., Fok, M.-C., Wolf, R. A., Thomsen, M. F., & Moore, T. E. 2005, *JGRA*, **110**, A02208
- Ebihara, Y., Hayakawa, H., Iwahashi, K., et al. 2017, *SpWea*, **15**, 1373
- Ebihara, Y., & Tanaka, T. 2021, *JGRA*, **126**, e28009
- Forbush, S. E. 1938, *TeMAE*, **43**, 203
- Forbush, S. E. 1946, *PhRv*, **70**, 771
- Gil, A., Kovaltsov, G. A., Mikhailov, V. V., et al. 2018, *SoPh*, **293**, 154
- Gilliland, T. R., Kirby, S. S., Smith, N., & Reymer, S. E. 1938, *Proceedings of the Institute of Radio Engineers*, **26**, 379
- Gonzalez, W. D., Joselyn, J. A., Kamide, Y., et al. 1994, *JGR*, **99**, 5771
- Gopalswamy, N., Yashiro, S., & Akiyama, S. 2007, *JGRA*, **112**, A06112
- Gopalswamy, N., Yashiro, S., Liu, Y., et al. 2005, *JGRA*, **110**, A09S15
- Hapgood, M. 2018, in *Extreme Space Weather: Origins, Predictability, and Consequences*, ed. N. Buzulukova (Amsterdam: Elsevier), 3
- Hapgood, M. 2019, *SpWea*, **17**, 950
- Hathaway, D. H. 2015, *LRSF*, **12**, 4
- Hattori, K., Hayakawa, H., & Ebihara, Y. 2019, *MNRAS*, **487**, 3550
- Haurwitz, M. W. 1968, *ApJ*, **151**, 351
- Hayakawa, H., Ebihara, Y., Pevtsov, A. A., et al. 2020a, *MNRAS*, **497**, 5507
- Hayakawa, H., Ebihara, Y., Willis, D. M., et al. 2018, *ApJ*, **862**, 15
- Hayakawa, H., Ebihara, Y., Willis, D. M., et al. 2019, *SpWea*, **17**, 1553
- Hayakawa, H., Iwahashi, K., Ebihara, Y., et al. 2017, *ApJL*, **850**, L31
- Hayakawa, H., Iwahashi, K., Tamazawa, H., et al. 2016, *PASJ*, **68**, 99
- Hayakawa, H., Ribeiro, J. R., Ebihara, Y., Correia, A. P., & Sôma, M. 2020c, *EP&S*, **72**, 122
- Hayakawa, H., Ribeiro, P., Vaquero, J. M., et al. 2020b, *ApJL*, **897**, L10
- Hess, V. F., Steinmaurer, R., & Demmelmair, A. 1938, *Natur*, **141**, 686
- I Drasis 1938, *Statements of specialists, I Drasis, 1938-1-28*, [in Greek]
- Jones, H. S. 1955, *Sunspot and Geomagnetic-Storm Data Derived from Greenwich Observations 1874-1954* (London: Her Majesty's Stationery Office)
- Kamide, Y., & Winningham, J. D. 1977, *JGR*, **82**, 5573
- Karafuto Department Observatory 1939, *Reports of the Polar Lights, Oturu, Taiyosha*, [in Japanese]
- Karinen, A., & Mursula, K. 2005, *JGRA*, **23**, 475
- Karinen, A., & Mursula, K. 2006, *JGRA*, **111**, A08207
- Kisho, Y. 1938a, *Kisho Yorán*, **462**, 127, [in Japanese]
- Kisho, Y. 1938b, *Kisho Yorán*, **463**, 226, [in Japanese]
- Knipp, D. J., Fraser, B. J., Shea, M. A., & Smart, D. F. 2018, *SpWea*, **16**, 1635
- Knipp, D. J., Ramsay, A. C., Beard, E. D., et al. 2016, *SpWea*, **14**, 614
- Korte, M., & Constable, C. 2011, *PEPI*, **188**, 247
- Kurochkin, N. 1939, *Bulletin of the Astronomical-Geodetical Society of the USSR*, **4**, 32, [in Russian]
- Lange, I., & Forbush, S. E. 1948, *Cosmic-Ray Results from Huancayo Observatory* (Washington, D.C.: Carnegie Institution of Washington Publication 175)
- Lefèvre, L., Vennerstrøm, S., Dumbović, M., et al. 2016, *SoPh*, **291**, 1483
- Lennahan, C. M. 1938, *MWRv*, **66**, 43
- Liu, Y. D., Zhao, X., Hu, H., Vourlidis, A., & Zhu, B. 2019, *ApJS*, **241**, 15
- Lockwood, M., Bentley, S. N., Owens, M. J., et al. 2019, *SpWea*, **17**, 180
- Love, J. J., Hayakawa, H., & Cliver, E. W. 2019, *SpWea*, **17**, 1281
- Lugaz, N., Farrugia, C. J., Huang, C.-L., & Spence, H. E. 2015, *GeoRL*, **42**, 4694
- Mannucci, A. J., Tsurutani, B. T., Iijima, B. A., et al. 2005, *GeoRL*, **32**, L12S02
- McCracken, K. G. 2007, *SpWea*, **5**, 07004
- McCracken, K. G., & Palmeira, R. A. R. 1960, *JGR*, **65**, 2673
- McIlwain, C. E. 1966, *Space Sci. Rev.*, **5**, 585
- Mekhaldi, F., Muscheler, R., Adolphi, F., et al. 2015, *NatCo*, **6**, 8611
- Meng, X., Tsurutani, B. T., & Mannucci, A. J. 2019, *JGRA*, **124**, 3926
- Miyake, F., Masuda, K., & Nakamura, T. 2013, *NatCo*, **4**, 1748
- Miyake, F., Nagaya, K., Masuda, K., & Nakamura, T. 2012, *Natur*, **486**, 240
- Miyake, F., Usoskin, I., & Poluianov, S. 2019, *Extreme Solar Particle Storms: The Hostile Sun* (Bristol: IOP Publishing)
- Moisejev, A. 1939a, *Bulletin of the Astronomical-Geodetical Society of the USSR*, **1**, 13, [in Russian]
- Moisejev, A. 1939b, *Bulletin of the Astronomical-Geodetical Society of the USSR*, **1**, 16, [in Russian]
- Morioka Observatory 1954, *Iwate Disaster Chronicle* (Morioka: Iwate Nippou) [in Japanese]
- Mursula, K., Holappa, L., & Karinen, A. 2008, *Astrophys. Space Sci. Trans. (ASTRA)*, **4**, 41
- O'Brien, B. J., Laughlin, C. D., van Allen, J. A., & Frank, L. A. 1962, *JGR*, **67**, 1209
- O'Brien, T. P., & McPherron, R. L. 2000, *GeoRL*, **27**, 3797
- Pevtsov, A. A., Tlatova, K. A., Pevtsov, A. A., et al. 2019, *A&A*, **628**, A103
- Poluianov, S. V., Usoskin, I. G., Mishev, A. L., Shea, M. A., & Smart, D. F. 2017, *SoPh*, **292**, 176
- Rastogi, R. G., Rao, D. R. K., Alex, S., Pathan, B. M., & Sastry, T. S. 1997, *AnGeo*, **15**, 1301
- Richardson, I. G., & Cane, H. V. 2010, *SoPh*, **264**, 189
- Richardson, I. G., Wibberenz, G., & Cane, H. V. 1996, *JGRA*, **101**, 13483
- Riley, P. 2017, in *Extreme Events in Geospace: Origins, Predictability, and Consequences*, ed. N. Buzulukova (Amsterdam: Elsevier), 115
- Riley, P., Baker, D., Liu, Y. D., et al. 2018, *SSRv*, **214**, 21
- Roach, F. E., Moore, J. G., Bruner, E. C., Jr., Cronin, H., & Silverman, S. M. 1960, *JGR*, **65**, 3575
- Sellers, B., Hanser, F. A., Stroschio, M. A., & Yates, G. K. 1977, *Radio Sci.*, **12**, 779
- Shea, M. A., & Smart, D. F. 2000, *SSRv*, **93**, 229
- Shea, M. A., & Smart, D. F. 2012, *SSRv*, **171**, 161
- Shea, M. A., & Smart, D. F. 2019, *ICRC* (Madison, WI), **36**, 1149
- Shiokawa, K., Ogawa, T., & Kamide, Y. 2005, *JGRA*, **110**, A05202
- Shiota, D., & Kataoka, R. 2016, *SpWea*, **14**, 56
- Silverman, S. M. 2006, *AdSpR*, **38**, 136
- Siscoe, G. L., & Christopher, L. 1975, *JGG*, **27**, 485
- Siscoe, G. L., Formisano, V., & Lazarus, A. J. 1968, *JGR*, **73**, 4869
- Slonim, Y.-M. 1939, *BTasO*, **2**, 37, [in Russian]
- Slonim, Y.-M., & Ushakova, E.-F. 1938, *BTasO*, **1**, 285, [in Russian]
- Smith, J. P., Thomsen, M. F., Borovsky, J. E., & Collier, M. 1999, *GeoRL*, **26**, 1797
- Steljes, J. F., Carmichael, H., & McCracken, K. G. 1961, *JGR*, **66**, 1363
- Stoker, P. H. 1995, *SSRv*, **73**, 327
- Störmer, C. 1938, *Natur*, **141**, 955
- Sudol, J. J., & Harvey, J. W. 2005, *ApJ*, **635**, 647
- Sugiura, M. 1964, *Ann. Int. Geophys. Year*, **35** (Oxford: Pergamon), 9
- Švestka, Z. 1966, *BAC*, **17**, 262
- Švestka, Z. 1976, *Solar Flares* (Berlin: Springer-Verlag)
- Thébault, E., Finlay, C. C., Beggan, C. D., et al. 2015, *EP&S*, **67**, 79
- The Christian Science 1938, *The Christian Science Monitor*, 1938-1-18, 2
- Thomsen, M. F., Borovsky, J. E., McComas, D. J., & Collier, M. R. 1998, *GeoRL*, **25**, 3481
- Tsurutani, B. T., Echer, E., Shibata, K., et al. 2014, *JSWSC*, **4**, A02
- Tsurutani, B. T., Gonzalez, W. D., Lakhina, G. S., & Alex, S. 2003, *JGRA*, **108**, 1268
- Tsurutani, B. T., & Lakhina, G. S. 2014, *GeoRL*, **41**, 287
- U.S. Department of Agriculture Weather Bureau 1938, *Climatological Data* (Washington DC: Department of Agriculture), 25
- Usoskin, I. G., Bazilevskaya, G. A., & Kovaltsov, G. A. 2011, *JGR*, **116**, A02104
- Usoskin, I. G., Berdyugina, S. V., Moss, D., & Sokoloff, D. D. 2007, *AdSpR*, **40**, 951
- Usoskin, I. G., Kromer, B., Ludlow, F., et al. 2013, *A&A*, **552**, L3
- Usoskin, I., Koldobskiy, S., Kovaltsov, G. A., et al. 2020a, *JGRA*, **125**, e27921
- Usoskin, I., Koldobskiy, S., Kovaltsov, G. A., et al. 2020b, *A&A*, **640**, A17

Wadsworth, J. 1938, [TeMAE](#), **43**, 186

Willever, J. C. 1938, [TeMAE](#), **43**, 178

WDC for Geomagnetism at Kyoto, Nose, M., Iyemori, T., Sugiura, M., & Kamei, T. 2015, [Geomagnetic Dst index](#),

Yokouchi, Y. 1953, *Memoirs of the Kakioka Magnetic Observatory*, **6**, 191, [in Japanese]

Yokoyama, N., Kamide, Y., & Miyaoka, H. 1998, [AnGeo](#), **16**, 566

Youssef, M. 2012, [JAsGe](#), **1**, 172